

Deformation behavior and indentation size effect in amorphous and crystallized Pd₄₀Cu₃₀Ni₁₀P₂₀ alloy

N. Li and L. Liu^{a)}

State Key Lab for Materials Processing and Die & Mold Technology, Huazhong University of Science and Technology, 430074 Wuhan, People's Republic of China

K.C. Chan

Department of Industrial and Systems Engineering, The Hong Kong Polytechnic University, Hong Kong, People's Republic of China

(Received 17 September 2008; accepted 17 November 2008)

The deformation behavior and indentation size effect (ISE) in amorphous and crystallized Pd₄₀Cu₃₀Ni₁₀P₂₀ alloy were comparatively studied through instrumented nanoindentation. It was found that the two alloys showed different deformation behaviors, the amorphous alloy exhibited conspicuous pop-in events in the load-depth (*P-h*) curve, while the crystallized alloy showed a relatively smooth *P-h* curve. In addition, the indentation hardness was observed to decrease with increasing penetration depth in the two alloys, exhibiting a significant ISE. However, the crystallized alloy displayed a sharper reduction of hardness with indentation depth as compared to the amorphous alloy, indicating a more significant indentation size effect in the crystalline alloy. The structure difference and friction factor associated with the surface residual stress are taken into account to interpret the difference in the deformation behavior and indentation size effect of the two alloys.

I. INTRODUCTION

Instrumented microindentation and nanoindentation techniques have been extensively used for the micromechanical characterization of materials due to their high time resolution and spatial resolution. However, the hardness is often found to decrease as the depth of penetration increases during indentation, that is, the so-called indentation size effect (ISE).¹ Upit and Varchenya² first investigated the ISE in single crystals and related it to the effect of free surface on the behavior of dislocations. Based on the Taylor dislocation and geometrically necessary dislocations (GNDs) induced by imposed strain gradients underneath an indenter, Nix and Gao^{3–5} developed the strain gradient plasticity (SGP) model that established a linear relationship between the square of hardness (H^2) and the reciprocal of the indentation depth (h^{-1}). However, this model is only applicable for indentation depth between 0.1–10 μm , but became invalid for an indentation depth of less than 100 nm.^{6,7} The improvements to the model were made by modifying the GND storage volume,⁸ considering the effect of work hardening⁹ and the limitation of the maximum allowable density of GNDs¹⁰ in the nanoscale. On the other hand, the role of friction between the indenter

facets and the test specimen has been proven crucial in crystalline materials, and the contribution of friction to the ISE is inversely related to the indentation size.^{11,12} Other factors, such as surface effect,¹³ structural nonuniformity of the deformed volume,¹⁴ mixed elastic and plastic deformation response of material,¹⁵ and so on, have also been proposed to illustrate the complicated nature of the ISE.

Although most of the mechanisms developed in crystalline materials are based on the dislocation theory, the ISE has also been reported recently in metallic glasses that lack dislocations. Wright et al.¹⁶ observed that the indentation hardness of Zr₄₀Ti₁₄Ni₁₀Cu₁₂Be₂₄ bulk metallic glass (BMG) decreases with increasing penetration depth, and attributed this result to the higher resistance of the BMG to the shear band nucleation at lower loads. Lam et al.¹⁷ proposed a strain gradient plasticity indentation model based on shear deformation clusters to elucidate the ISE. Yang et al.,¹⁸ on the other hand, argued that the ISE of BMG is caused by the generation of strain gradient due to the introduction of excessive free volume underneath the indenter, which results in strain softening.^{19–21} More recently, Li et al.²² found that the friction between the indenter facets and the test specimen also plays an important role for the ISE in Pd₄₀Cu₃₀Ni₁₀P₂₀ BMG.

To investigate the ISE in amorphous and crystalline materials, Manika et al.² studied the Vickers indentation

^{a)}Address all correspondence to this author.
e-mail: lliu2000@mail.hust.edu.cn
DOI: 10.1557/JMR.2009.0222

response in single crystals, polycrystals, and amorphous solids, and found that a significant ISE was clearly observed in single crystals and amorphous solids, but ISE was absent in fine-grained polycrystals. However, the mechanism for the ISE in amorphous and crystallized alloys has not been clearly understood. In this work, the ISE was investigated in amorphous and crystallized Pd₄₀Cu₃₀Ni₁₀P₂₀ alloys under different loads (corresponding to different penetration depths). It is shown that the two alloys exhibit quite different deformation behavior and also different indentation size effect.

II. EXPERIMENTAL PROCEDURE

The amorphous Pd₄₀Cu₃₀Ni₁₀P₂₀ cylindrical rod with a diameter of 12 mm was prepared by water quenching of the alloy melt in a sealed quartz tube. The crystallized sample was prepared by annealing the amorphous alloy at 423 °C for 48 h in vacuum. The structure of the as-cast and of the annealed samples was examined by x-ray diffraction (XRD, Philips X'Pert PRO, Eindhoven, The Netherlands) and differential scanning calorimetry (DSC, Perkin-Elmer DSC-7, USA).

Nanoindentation experiments were carried out using a Triboindenter instrumented nanoindenter (from Hysitron, Minneapolis, MN) with a Berkovich diamond indenter, calibrated using pure aluminum and silica. In all the experiments, the temperature and air humidity inside the apparatus chamber were kept constant. Prior to nanoindentation, the surfaces of the samples were carefully polished to a mirror finish. The indentations were performed under load control at a loading rate of 0.5 mN s⁻¹. To obtain different indentation depths, samples were loaded under different maximum loads (P_{max}) ranging from 2 to 10 mN. At least six indents were made at each load to verify the accuracy and scatter of the indentation data.

To observe the deformation patterns beneath the nanoindenter tip in amorphous and crystallized alloys, a bonded interface technique was used and the nanoindentation was exactly performed at the interface of each alloy with the guidance of the atom force microscope. The details of the technique were described elsewhere.²² The indent morphology was then examined by scanning electron microscopy (SEM, JEOL JSM-6335F, Tokyo, Japan).

III. RESULTS

Figure 1(a) shows the XRD patterns obtained from the as-cast and annealed Pd₄₀Cu₃₀Ni₁₀P₂₀ alloy. The as-cast alloy is clearly of amorphous structure characterized by only a broad diffraction hump in its XRD pattern, while the annealed one is fully crystallized as indicated by a series of diffraction peaks indexed as Ni₂Pd₂P and P_{3.2}Pd₁₂ intermetallic compounds. The different structure of the two alloys was further verified by DSC scans

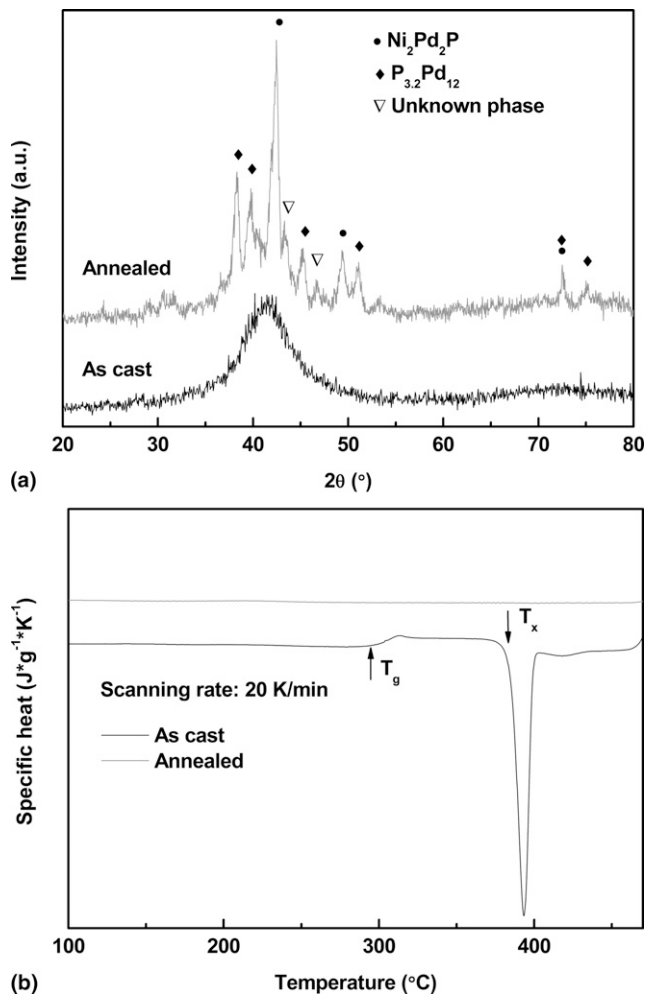


FIG. 1. (a) XRD patterns and (b) DSC scans of as-cast and annealed Pd₄₀Cu₃₀Ni₁₀P₂₀ alloys.

as shown in Fig. 1(b), in which the as-cast alloy exhibits a distinct glass transition and subsequent crystallization, while the glass transition and crystallization signals completely disappeared in the annealed alloy.

Figure 2 shows the typical load-depth ($P-h$) curves for the amorphous and crystallized Pd₄₀Cu₃₀Ni₁₀P₂₀ alloys, respectively, obtained under an applied load of 10 mN at a loading rate of 0.5 mN s⁻¹. It is noted that the $P-h$ curves show strong structure dependence. In the amorphous alloy there is a lack of dislocations, the $P-h$ curve is punctuated by a number of discrete bursts of pop-ins, indicative of the nucleation of shear bands.¹⁶ In contrast, the crystallized alloy exhibits a relatively smooth $P-h$ curve under the same experimental conditions. However, the enlargement of the $P-h$ curve for the crystallized alloy also clearly shows a few serrations with a small pop-in size due to the initiation of dislocations,²³ as described in the inset in Fig. 2.

Figures 3(a) and 3(b) illustrate the deformation patterns underneath nanoindents in the amorphous and

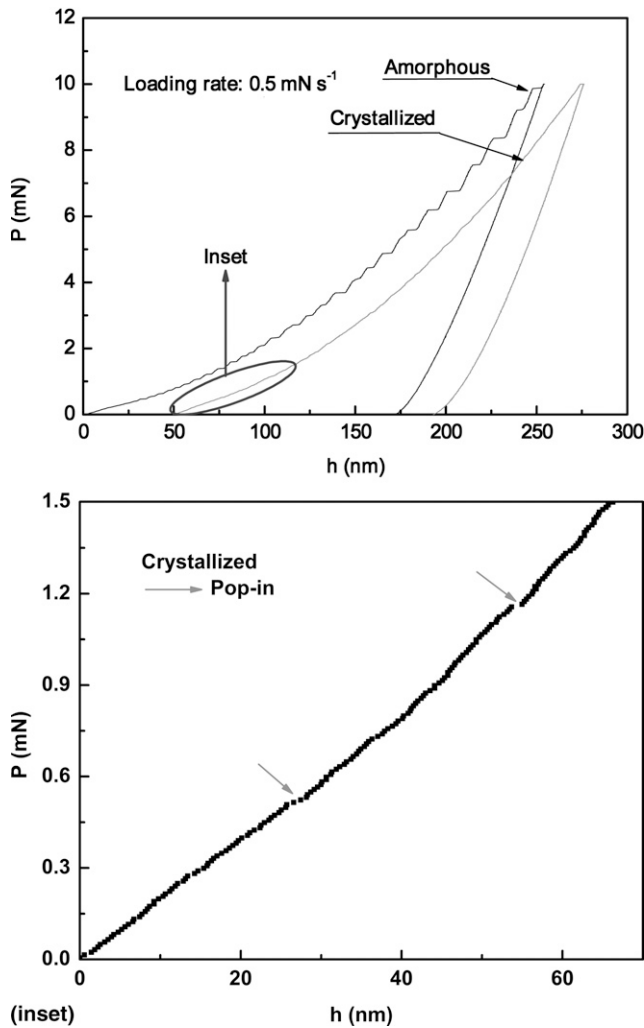
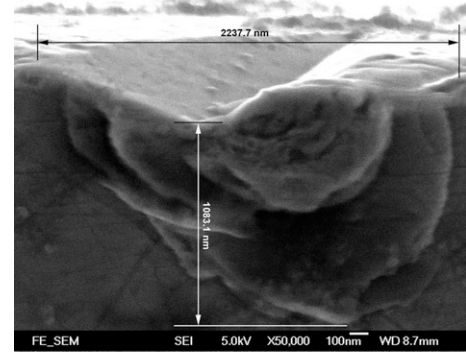


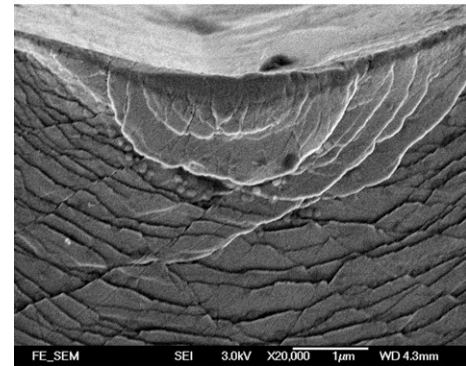
FIG. 2. Typical load-depth ($P-h$) curves of the amorphous and crystallized Pd₄₀Cu₃₀Ni₁₀P₂₀ alloy obtained under load of 10 mN. The inset shows the enlargement of $P-h$ curves of the crystallized alloy under 1.5 mN.

crystallized Pd₄₀Cu₃₀Ni₁₀P₂₀ alloy at an applied load of 10 mN. A notable difference in the band patterns can be clearly observed in the two alloys. The semicircular shear bands in the amorphous alloy are clearly larger than the values of the slip bands in the crystallized alloy. To further understand the difference in the deformation behavior in amorphous and crystallized Pd₄₀Cu₃₀Ni₁₀P₂₀ alloys, the two alloys were also examined under micro-indentation using a Vickers indenter under a load of 1000 mN. The deformation pattern is shown in the inset of Fig. 3. It can be seen clearly that the deformation region in the amorphous alloy contains a high density of shear bands. However, only a few slip bands, with cracks at the edge of the indentation, are observed in the crystallized alloy.

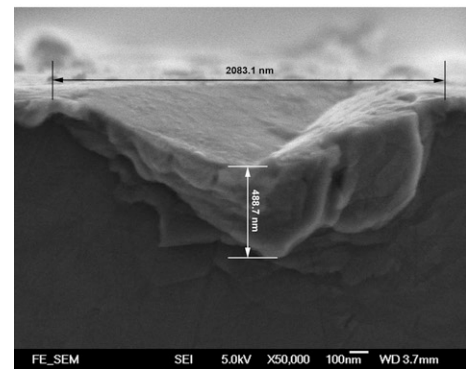
Figure 4 shows the variation of the nanoindentation hardness (H) as a function of the maximum penetration depth (h_{max}), where H is calculated from the Oliver-



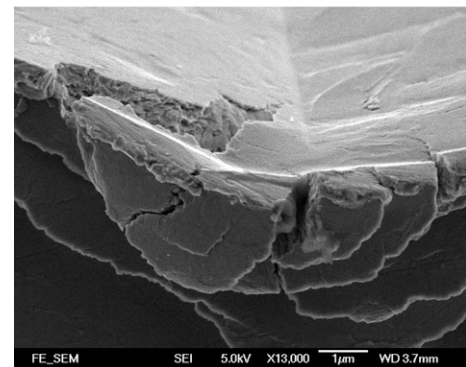
(a)



(a) (inset)



(b)



(b) (inset)

FIG. 3. SEM images of the subsurface deformation regions for (a) amorphous and (b) crystallized Pd₄₀Cu₃₀Ni₁₀P₂₀ alloy obtained under nanoindentation (10 mN). The inset shows the corresponding SEM images obtained under micro indentation (1000 mN).

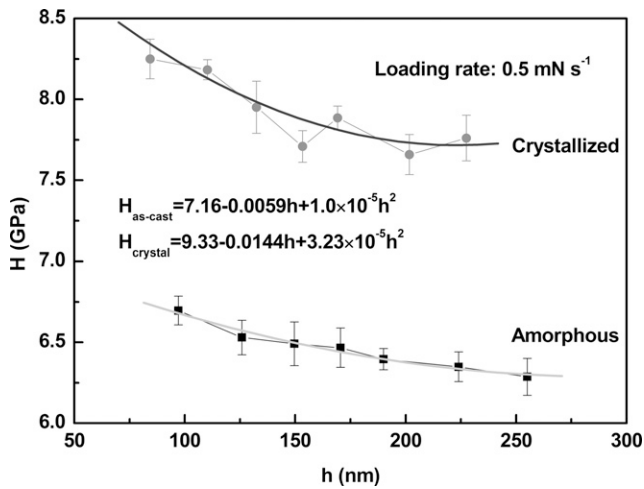


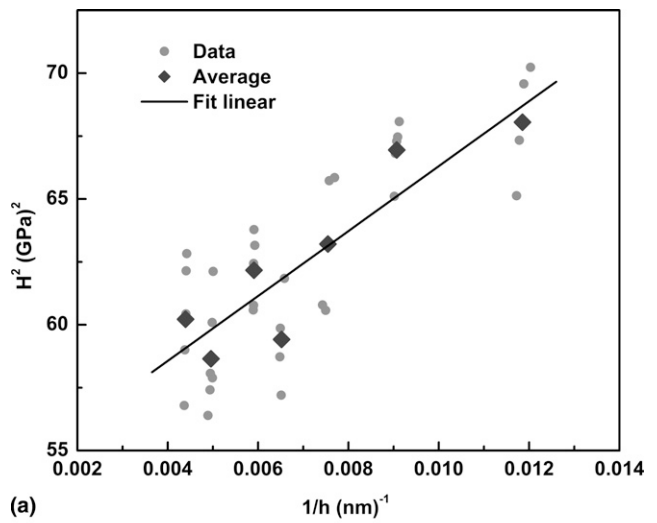
FIG. 4. Dependence of the indentation hardness on depth for amorphous and crystallized Pd₄₀Cu₃₀Ni₁₀P₂₀ alloys.

Pharr approach.²⁴ It can be clearly seen that the indentation hardness in both the amorphous and crystallized Pd₄₀Cu₃₀Ni₁₀P₂₀ alloys decreases with the increase in penetration depth. This demonstrates a significant ISE. However, it can be also observed in Fig. 4 that the crystallized alloy displays a sharper reduction of hardness with indentation depth, as compared with amorphous alloy, indicating a more significant indentation size effect in the crystalline alloy.

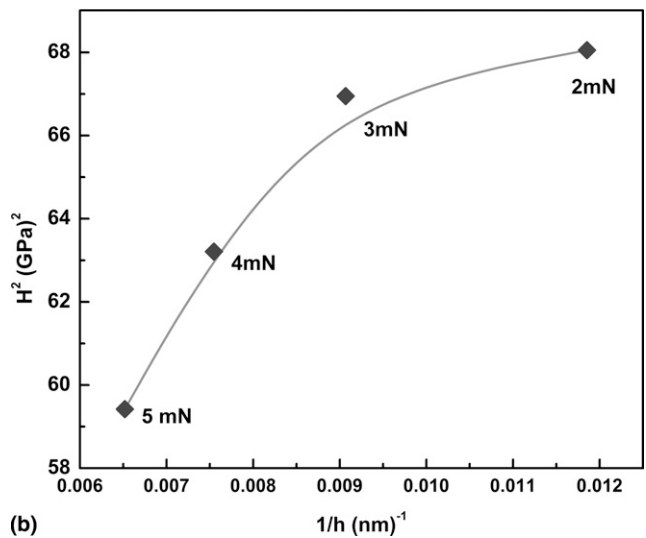
IV. DISCUSSION

The pop-in events in *P-h* curves during nanoindentation have been extensively reported in a number of crystalline materials and are widely recognized as an important indicator of the initiation of dislocations at the critical shear stresses.^{25,26} The size of the pop-ins is considered proportional to the displacement of the slip. The small pop-in size observed in the crystallized Pd₄₀Cu₃₀Ni₁₀P₂₀ alloy in the study indicates that the dislocations glide only a short distance before being blocked by grain boundaries. In contrast, the deformation in amorphous alloys is usually localized in a few thin shear bands,²⁷ and the nucleation and propagation of shear bands is generally regarded as the main cause for the pop-in events in the *P-h* curves during nanoindentation.²⁸ The size of pop-ins in the amorphous Pd₄₀Cu₃₀Ni₁₀P₂₀ alloy increases with the indentation depths, which can be attributed to the greater shear displacements within larger shear bands in deeper indentation depths.²⁹

The ISE in crystalline metals has been explained by various theories, the most popular being the model of strain gradient plasticity (SGP) proposed by Nix and Gao.³⁻⁵ According to this model, the total dislocation density (ρ_T) can be expressed by $\rho_T = \rho_S + \rho_G(h^*/h)$, where ρ_S is the density of statistically stored disloca-



(a)



(b)

FIG. 5. (a) Average value of H^2 as a function of $1/h$ for crystallized Pd₄₀Cu₃₀Ni₁₀P₂₀ alloy. (b) Shows the fit curve under loads ranging from 2 to 5 mN.

tions, ρ_G is the geometrically necessary dislocations, and h^* is a characteristic depth. At small indentation depths ($h < h^*$), the density of geometrically necessary dislocations (GNDs) that is proportional to the strain gradient becomes appreciable.³⁰ On the basis of the GND model, the hardness and indentation depth have the following relationship:

$$H = H_0 \sqrt{1 + \frac{h^*}{h}} \quad (1)$$

where H_0 is the indentation hardness for a large indentation depth (i.e., $h \gg h^*$). According to Eq. (1), the plot of H^2 against h^{-1} for the crystallized Pd₄₀Cu₃₀Ni₁₀P₂₀ alloy can be obtained, as described in Fig. 5. It can be seen that the datum distribute discretely along the fit line. It is believed that the significant scattering of the data is attributed to the inhomogeneous microstructure in the

polycrystalline alloy, which involves a lot of crystalline defects, such as grain boundaries. However, if one follows the average value of the hardness at the load from 2 to 5 mN (corresponding to various indentation depths), a parabolic H^2 versus h^{-1} curve was can be obtained, as shown in Fig. 5(b). The deviation from the linear relationship between hardness and the indentation depth indicates that the SGP model as a simplified approach is insufficient to elucidate such a complicated ISE.

In the case of an amorphous alloy that does not involve any dislocations, it has been reported that plastic flow is associated with dilatation due to the creation of excessive free volume in shear bands.²⁷ This leads to strain softening and causes the reduction of hardness with increasing indentation depth, that is, ISE.^{18,21} According to Spaepen's general flow equation,²⁷ the shear strain rate ($\dot{\gamma}$) in metallic glass can be expressed as:

$$\dot{\gamma} = 2\nu\Delta f c_f \sinh\left(\frac{\tau\Omega}{2k_B T}\right) \exp\left(-\frac{\Delta G}{k_B T}\right), \quad (2)$$

where ν is the frequency of atomic vibration (i.e., the Debye frequency), Δf is the fraction of the sample volume in which potential jump sites can be found, c_f is the defect concentration, which is exponentially proportional to the reciprocal of the reduced free volume (x), that is, $c_f = \exp(-1/x)$.²¹ τ is the shear stress, which is proportional to the indentation hardness by $H \approx 3\sqrt{3}\tau$,²¹ Ω is the atom volume, k_B is the Boltzmann constant, T is the test temperature, and ΔG is the activation barrier energy for defect migration. During plastic deformation, the shear strain rate ($\dot{\gamma}$) can also be expressed as $\dot{\gamma} = 0.16\dot{\epsilon}_i = 0.16\frac{1}{h}\frac{dh}{dt}$.³¹ The dependence of $\dot{\gamma}$ on h during loading is plotted in Fig. 6(a), from which one can conclude that shear strain rate $\dot{\gamma}$ is almost identical and can be regarded as a constant at the ending stage for each applied load. Assuming Δf and ΔG remain constant during nanoindentation, Eq. (2) can be rewritten as:

$$Kc_f \approx \frac{1}{H}, \quad (3)$$

where $K = \frac{\sqrt{3}}{9}\nu\Delta f\frac{\Omega}{k_B T\dot{\gamma}}\exp\left(-\frac{\Delta G}{k_B T}\right)$ is regarded as a constant. On the basis of the Eq. (3), a plot of Kc_f against h can be obtained and is shown in Fig. 6(b), which demonstrates that the defect concentration (corresponding the free volume) during nanoindentation increases monotonically with increasing indent depth.

It is expected that the friction between the indentation facets and the test specimen also plays an important role in the indentation size effect, which is usually analyzed quantitatively through a proportional specimen

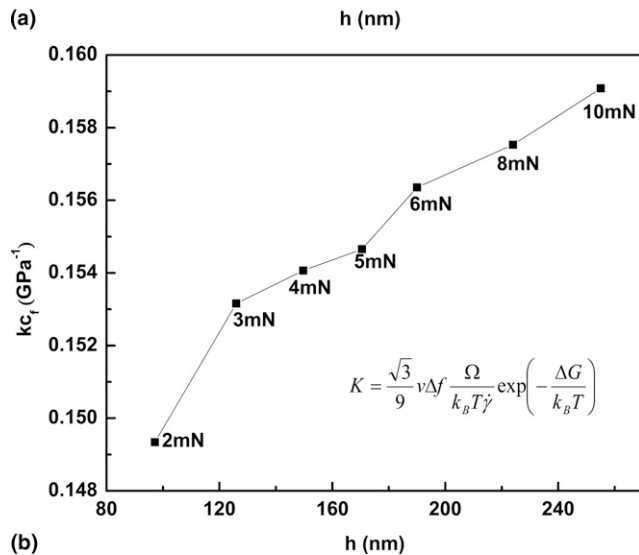
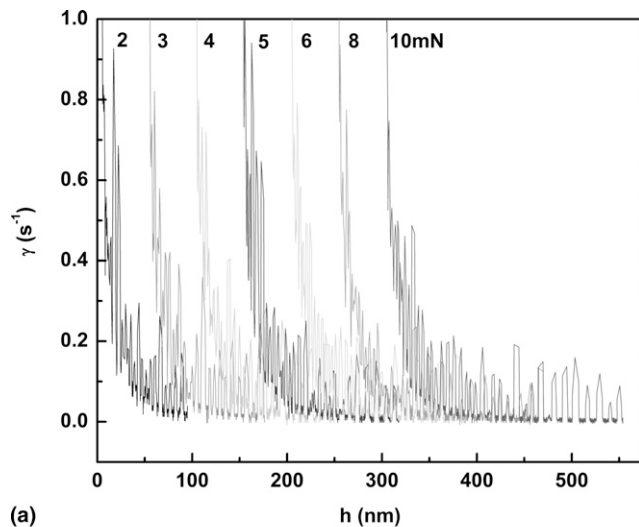


FIG. 6. (a) Dependence of the shear strain rate ($\dot{\gamma}$) on the penetration depth and the (b) estimation of free volume created during indentation for as-cast Pd₄₀Cu₃₀Ni₁₀P₂₀ BMG.

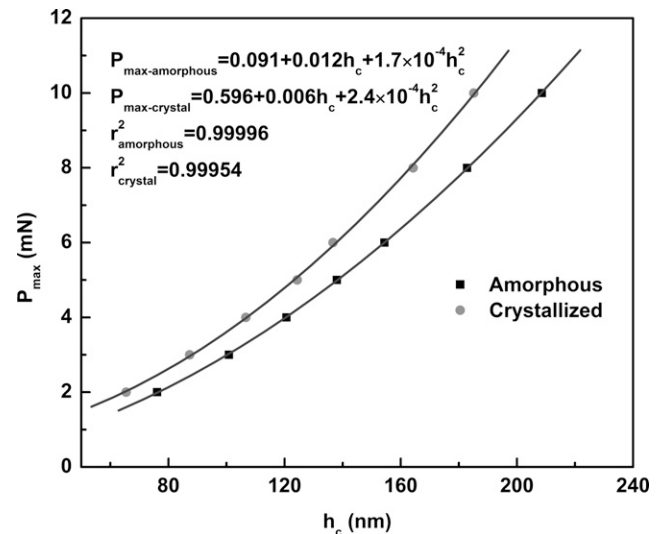


FIG. 7. The modified proportional specimen resistance (PSR) model applied to the amorphous and crystallized Pd₄₀Cu₃₀Ni₁₀P₂₀ alloys.

resistance (PSR) model.^{11,32,33} Considering that the surface residual stress is associated with the surface machining and polishing,³⁴ a modified form of the PSR model is used in the present work, which is given in Eq. (4):

$$P_{\max} = a_0 + a_1 h_c + a_2 h_c^2, \quad (4)$$

where P_{\max} is the indentation test load, h_c is the plastic indentation depth, a_0 is a constant related to the surface residual stresses, a_1 is the coefficient describing the proportional specimen resistance (the friction between the indenter facets and the test specimen), and a_2 is the coefficient that is related to the load-independent hardness.^{35,36} The application of Eq. (4) to the data in the present alloys yields plots of P_{\max} versus h_c with a high correction coefficient ($r^2 > 0.9995$), as shown in Fig. 7. This suggests that the modified PSR model can elucidate well the ISE of amorphous and crystallized Pd₄₀Cu₃₀Ni₁₀P₂₀ alloys. Interestingly, the fitting function of P_{\max} - h_c curves in Fig. 7 shows a higher value of a_0 for the crystalline alloy (~0.596), which is almost 6.6 times larger than that for the amorphous alloy. The result indicates that the crystalline alloy has a higher surface residual stress, which in turn results in a more significant ISE in the crystalline alloy as compared to the amorphous alloy.

V. CONCLUSIONS

The deformation behavior and indentation size effect of amorphous and crystallized Pd₄₀Cu₃₀Ni₁₀P₂₀ alloy were investigated through instrumented nanoindentation. The results demonstrate a different deformation behavior in the two alloys. The amorphous alloy exhibited prominent pop-in events in the P - h curve, but the crystallized alloy showed a relatively smooth P - h curve. The different deformation behavior is attributed to the different microstructures of the two alloys, that is, the propagation of shear bands dominates the large serrations in the amorphous alloy, while the sliding of dislocations governs the small pop-in event in the fine-grained crystalline alloy. In addition, the two alloys demonstrate a quite different indentation size effect (ISE). The crystallized alloy exhibited a more significant ISE with respect to the amorphous alloy. The difference is attributed to the residual surface effects caused by surface machining and polishing.

ACKNOWLEDGMENTS

This work was financially supported by the National Nature Science Foundation of China under Grant No. 50635020. The work was also partially supported by the funding from the Department of Industrial System and Engineering, the Hong Kong Polytechnic University. The authors are grateful to the Analytical and Testing Center, Huazhong University of Science and Technology for technical assistance.

REFERENCES

- S.S. Joshi and S.N. Melkote: An explanation for the size effect in machining using strain gradient plasticity. *J. Manuf. Sci. Eng.* **126**, 679 (2004).
- I. Manika and J. Maniks: Size effects in micro- and nanoscale indentation. *Acta Mater.* **54**, 2049 (2006).
- W.D. Nix and H. Gao: Indentation size effects in crystalline materials: A law for strain gradient plasticity. *J. Mech. Phys. Solids* **46**, 411 (1998).
- H. Gao, Y. Huang, and W.D. Nix: Modeling plasticity at the micrometer scale. *Naturwissenschaften* **86**, 507 (1999).
- H. Gao, Y. Huang, W.D. Nix, and J.W. Hutchinson: Mechanism-based strain gradient plasticity—I. Theory. *J. Mech. Phys. Solids* **47**, 1239 (1999).
- J.G. Swadener, E.P. George, and G.M. Pharr: The correlation of the indentation size effect measured with indenters of various shapes. *J. Mech. Phys. Solids* **50**, 681 (2002).
- J.Y. Kim, B.W. Lee, D.T. Read, and D. Kwon: Influence of tip bluntness on the size-dependent nanoindentation hardness. *Scr. Mater.* **52**, 353 (2005).
- G. Feng and W.D. Nix: Indentation size effect in MgO. *Scr. Mater.* **51**, 599 (2004).
- J.G. Swadener, A. Misra, R.G. Hoagland, and M. Nastasi: A mechanistic description of combined hardening and size effects. *Scr. Mater.* **47**, 343 (2002).
- Y. Huang, F. Zhang, K.C. Hwang, W.D. Nix, G.M. Pharr, and G. Feng: A model of size effects in nano-indentation. *J. Mech. Phys. Solids* **54**, 1668 (2006).
- H. Li, A. Ghosh, Y.H. Han, and R.C. Bradt: The frictional component of the indentation size effect in low load microhardness testing. *J. Mater. Res.* **8**, 1028 (1993).
- M. Atkinson: Further analysis of the size effect in indentation hardness tests of some metals. *J. Mater. Res.* **10**, 2908 (1995).
- W.W. Gerberich, N.I. Tymiak, J.C. Grunlan, M.F. Horstemeyer, and M.I. Baskes: Interpretations of indentation size effects. *J. Appl. Mech.* **69**, 433 (2002).
- J. Skinner and N. Gane: Sliding friction under a negative load. *J. Phys. D: Appl. Phys.* **5**, 2087 (1972).
- S.J. Bull, T.F. Page, E.H. Yoffe, S.J. Bull, T.F. Page, and E.H. Yoffe: An explanation for the indentation size effect in ceramics. *Philos. Mag. Lett.* **59**, 281 (1989).
- W.J. Wright, R. Saha, and W.D. Nix: Deformation mechanisms of the Zr₄₀Ti₁₄Ni₁₀Cu₁₂Be₂₄ bulk metallic glass. *Mater. Trans.* **42**, 642 (2001).
- D.C.C. Lam and A.C.M. Chong: Model and experiments on strain gradient hardening in metallic glass. *Mater. Sci. Eng., A* **318**, 313 (2001).
- F.Q. Yang, K.B. Geng, P.K. Law, G.J. Fan, and H. Choo: Deformation in a Zr₅₇Ti₅Cu₂₀Ni₈Al₁₀ bulk metallic glass during nanoindentation. *Acta Mater.* **55**, 321 (2007).
- A. Concustell, J. Sort, G. Alcalá, S. Mato, A. Gebert, J. Eckert, and M.D. Baró: Plastic deformation and mechanical softening of Pd₄₀Cu₃₀Ni₁₀P₂₀ bulk metallic glass during nanoindentation. *J. Mater. Res.* **20**, 2719 (2005).
- H. Bei, S. Xie, and E.P. George: Softening caused by profuse shear banding in a bulk metallic glass. *Phys. Rev. Lett.* **96**, 105503 (2006).
- N. Van Steenberge, J. Sort, A. Concustell, J. Das, S. Scudino, S. Suriñach, J. Eckert, and M.D. Baró: Dynamic softening and indentation size effect in a Zr-based bulk glass-forming alloy. *Scr. Mater.* **56**, 605 (2007).
- N. Li, K.C. Chan, and L. Liu: The indentation size effect in Pd₄₀Cu₃₀Ni₁₀P₂₀ bulk metallic glass. *J. Phys. D: Appl. Phys.* **41**, 155415 (2008).

23. J.E. Bradby, S.O. Kucheyev, J.S. Williams, J. Wong-Leung, M.V. Swain, P. Munroe, G. Li, and M.R. Phillips: Indentation-induced damage in GaN epilayers. *Appl. Phys. Lett.* **80**, 383 (2002).
24. W.C. Oliver and G.M. Pharr: Measurement of hardness and elastic modulus by instrumented indentation: Advances in understanding and refinements to methodology. *J. Mater. Res.* **7**, 1564 (1992).
25. S.O. Kucheyev, J.E. Bradby, J.S. Williams, C. Jagadish, and M.V. Swain: Mechanical deformation of single-crystal ZnO. *Appl. Phys. Lett.* **80**, 956 (2002).
26. C.A. Schuh, J.K. Mason, and A.C. Lund: Quantitative insight into dislocation nucleation from high-temperature nanoindentation experiments. *Nat. Mater.* **4**, 617 (2005).
27. F. Spaepen: A microscopic mechanism for steady state inhomogeneous flow in metallic glasses. *Acta Metall.* **25**, 407 (1977).
28. T. Burgess, K.J. Laws, and M. Ferry: Effect of loading rate on the serrated flow of a bulk metallic glass during nanoindentation. *Acta Mater.* **56**, 4829 (2008).
29. C.A. Schuh and T.G. Nieh: A nanoindentation study of serrated flow in bulk metallic glasses. *Acta Mater.* **51**, 87 (2003).
30. Y.G. Wei, X.Z. Wang, and M.H. Zhao: Size effect measurement and characterization in nanoindentation test. *J. Mater. Res.* **19**, 208 (2004).
31. C.A. Schuh, A.C. Lund, and T.G. Nieh: New regime of homogeneous flow in the deformation map of metallic glasses: Elevated temperature nanoindentation experiments and mechanistic modeling. *Acta Mater.* **52**, 5879 (2004).
32. H. Shi and M. Atkinson: A friction effect in low-load hardness testing of copper and aluminium. *J. Mater. Sci.* **25**, 2111 (1990).
33. H. Li and R.C. Bradt: The microhardness indentation load/size effect in rutile and cassiterite single crystals. *J. Mater. Sci.* **28**, 917 (1993).
34. J.H. Gong, J.J. Wu, and Z.D. Guan: Examination of the indentation size effect in low-load vickers hardness testing of ceramics. *J. Eur. Ceram. Soc.* **19**, 2625 (1999).
35. O. Şahin, O. Uzun, U. Kölemen, and U. Uçar: analysis of ISE in dynamic hardness measurements of β -Sn single crystals using a depth-sensing indentation technique. *Mater. Charact.* **59**, 729 (2008).
36. Z.J. Peng, J.H. Gong, and H.Z. Miao: On the description of indentation size effect in hardness testing for ceramics: Analysis of the nanoindentation data. *J. Eur. Ceram. Soc.* **24**, 2193 (2004).